Separation Science and Technology
Publication details, including instructions for authors and subscription information:
http://www.informaworld.com/smpp/title~content=t713708471

Drop-Interface Coalescence Rate in Tertiary Amine Solvent Extraction

Bruce Mover[a]; W. J. McDowell[a]
[a] Oak Ridge National Laboratory, Oak Ridge, Tennessee

To cite this Article Mover, Bruce and McDowell, W. J.(1983) 'Drop-Interface Coalescence Rate in Tertiary Amine Solvent Extraction', Separation Science and Technology, 18: 14, 1535 — 1562
To link to this Article: DOI: 10.1080/01496398308056114
URL: http://dx.doi.org/10.1080/01496398308056114

SEPARATION SCIENCE AND TECHNOLOGY, 18(14&15), pp. 1535-1562, 1983

Drop-Interface Coalescence Rate In Tertiary Amine Solvent Extraction

BRUCE MOYER and W. J. McDOWELL

OAK RIDGE NATIONAL LABORATORY
P. O. BOX X
OAK RIDGE, TENNESSEE 37830

ABSTRACT

An important requirement for economical application of solvent extraction technology is rapid and efficient phase disengagement. However, much progress toward a clear fundamental understanding of the factors that affect phase disengagement rate will be needed before a logical approach to the problem will be possible. In this paper, we develop the conceptual framework for the study of drop-interface coalescence in collapsing liquid/liquid dispersions and present the details of the experimental setup employed in our initial work. The method for determining the drop-interface coalescence rate requires measurement of the average volume of drops ($\bar{v}_f$) adjacent to the interface, their number (n) per unit area of interface, and dispersed-phase throughput (Q) per unit area. We have employed recording videomicrography for measurement of $\bar{v}_f$ and n, while Q is found from the changing position of the major interface as the dispersion band collapses (batch mode).

Experimental results are presented for the highly purified system 0.1 M trioctylamine in o-xylene vs 0.1 M HCl, 0.9 M LiCl. Successive batch phase-mixing runs (1:1 phase ratio) using this system produced highly reproducible results, attributed to the use of high-purity chemicals and noncontaminating cell construction materials. Wall effects were found to be negligible. The results indicated that the changing throughput observed in batch experiments is brought about not only by drop size growth rates, but also by drop packing behavior and the fact that drop-interface coalescence rate changes with time. Drop-interface coalescence rate was observed to increase from 0.16 to a maximum value of 0.95 s^{-1} at 49 s (break occurred at 63 s). The collapse of the disper-

 0149-6385/84/1814-1535$3.50/0

sion band was qualitatively described in terms of five separate stages based on throughput behavior and the patterns of drop growth and drop-interface coalescence rate.

INTRODUCTION

In the general sense, the rate at which a solvent extraction operation may be carried out is controlled by both a mass transfer step and a phase separation step. Good economics, therefore, dictates that phase separation be made as rapid and efficient as possible without jeopardizing system performance in other respects. Since the principal variable in the design of solvent extraction systems lies in the choice of extraction reagents, it was our original idea that the structure of the extraction reagent would possibly provide a means of controlling phase disengagement rate just as it permits control of extraction selectivity and mass transfer rate. To test this idea, we recently studied the phase disengagement behavior of a series of tertiary amine extractants using break time (time for complete separation of a uniform dispersion into two discrete bulk phases) as an indicator of overall performance (1). It was found that break time is highly dependent on the molecular structure of the amine, dispersion type (organic- vs aqueous-continuous), and the presence of interface-active suspended solids such as colloidal silica. Other factors known to be important include diluent type, aqueous acid type, diluent additives, amine concentration, and temperature (but curiously, not mixer energy input) (2,3). Although break time is a useful gross indicator of trends in phase disengagement behavior, it provides limited insight into the underlying processes involved. Therefore, to understand the trends we and others have observed, we have been taking a more mechanistic approach, seeking to understand the component processes that together constitute phase disengagement.

Since it is well known from emulsion science and technology (4) that interface-active substances strongly influence coalescence rates, we have been led to study drop coalescence as an avenue

toward understanding and predicting chemical influences on phase disengagement behavior. Although single-drop experiments have often been applied to this problem in the past (5,6), it was our thought that the study of drop coalescence phenomena in dispersions would yield a more immediate understanding of phase disengagement and would perhaps prove less susceptible to problems with purity and reproducibility. Hence, we have sought a means of determining coalescence rates in liquid/liquid mixing experiments. Such measurements are expected to provide an insightful way to test the ideas, assumptions, and models put forth previously (7-11) and to serve as a useful comparison of the effects of systematic molecular variations in extraction reagents and other chemical constituents.

In this paper, we describe our experimental approach to the determination of drop-interface (DI) coalescence rates in coalescing liquid/liquid dispersions. At the heart of the method is the quantitative relationship between dispersed-phase throughput and the size, packing, and coalescence rate of drops at the major interface. We develop this relationship explicitly since the literature has been, at best, sketchy. In addition to our measurement technique involving videomicrography, we present the results of our first complete batch experiment using purified 0.1 M trioctylamine (TOA) in o-xylene as the organic phase and 0.1 M HCl, 0.9 M LiCl as the aqueous phase. As such, it is not yet possible to compare chemical effects on coalescence, but some interesting mechanistic insights have been obtained regarding DI coalescence rate in batch phase disengagement.

MATHEMATICAL DEVELOPMENT

In this section, the objective is to derive an equation which gives the DI coalescence rate as a function of experimentally accessible variables such as drop diameter and dispersed-phase throughput. This will be presented in such a way as to show the clear connection to equations given elsewhere. We will consider

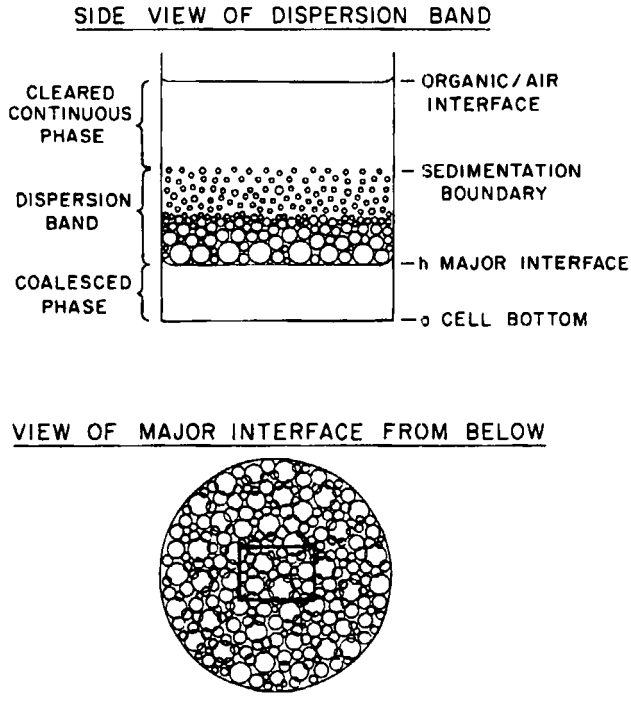

FIGURE 1. Organic-Continuous Dispersion Band. This pictorial representation (not actual data) of a dispersion band undergoing phase disengagement illustrates two possible zones within the band: a fluidized zone and a compact (lower) zone. During batch tests, the level h of the aqueous/organic interface ("major interface") moves upward as the sedimentation boundary moves downward. In continuous flow situations, the dimensions and zones of the band remain constant. The lower illustration represents how the major interface appears from below the cylindrical cell. In the center is shown the rectangle of arbitrary area A in which drops are counted and measured on the CCTV monitor.

the case of an organic-continuous dispersion band with uniform thickness as depicted in Fig. 1. Two discrete boundaries are typically observed (7). At the major interface, active DI coalescence occurs, whereas the sedimentation boundary passively divides the top of the dispersion band from the continuous organic phase that has been squeezed upward and out. We begin by assuming

the existence of large numbers of drops which may be described (at least for the sake of discussion) by continuous size-distribution functions. The analysis requires a constant drop-size distribution at any given time over the entire area of the major interface, and thus, wedge-type settling schemes are not considered. Further, secondary droplet formation and drop-wall coalescence are neglected.

In general, the layer of drops at the interface will exhibit a distribution of drop sizes as shown in Fig. 1. The number n of drops per unit area directly adjacent to the interface ("first-layer drops") at any time t may be expressed in terms of a distribution function f(v) summed over all possible drop volumes v per unit area:

$$n = \int_o^\infty f(v)dv \quad . \tag{1}$$

Thus, the number dn of drops of volume v (i.e., in the interval v to v + dv) per unit area is

$$dn = f(v)dv \quad . \tag{2}$$

The number of drops of volume v undergoing DI coalescence per unit area per second may be expressed as k(v)dn or k(v)f(v)dn, where k(v) is the coalescence frequency (units are s^{-1}) defined as the fraction of first-layer drops of volume v undergoing DI coalescence per unit area per second. Theoretical and experimental results lead to the expectation that k(v) varies as a function of v (6). Summing over all drop volumes gives the per-unit-area rate of disappearance of the total number N of drops in the dispersion band over unit area by the mechanism of DI coalescence:

$$-\left(\frac{dN}{dt}\right)_{DI} = \int_{v=o}^{v=\infty} k(v)dn = \int_o^\infty k(v)f(v)dv \quad . \tag{3}$$

Let $\bar{k}$ be the average DI coalescence frequency averaged over the distribution of first-layer drops:

$$\bar{k} = \frac{\int_0^\infty k(v)f(v)dv}{\int_0^\infty f(v)dv} \quad . \tag{4}$$

Substituting eqs. 1 and 4 into eq. 3 gives

$$-\left(\frac{dN}{dt}\right)_{DI} = \bar{k} \int_0^\infty f(v)dv = \bar{k}n \quad . \tag{5}$$

This expression represents the drop-interface coalescence portion of the deterministic model given by Vijayan and Ponter (9). It states that the instantaneous rate of disappearance of drops due to DI coalescence is proportional to the number of drops per unit area, where the factor $\bar{k}$ represents the fraction of all first-layer drops coalescing per second.

The average DI coalescence frequency $\bar{k}$ may be related to dispersed-phase throughput $Q = -\frac{dV}{dt}$ per unit area, where V is the total volume of dispersed phase per unit area at time t by considering the case for a particular drop volume. Since the total number of drops of volume v coalescing per second per unit area is k(v)dn, the total volume of all drops of volume v DI-coalescing per unit area per second must be vk(v)dn or vk(v)f(v)dv. Summing over all drop volumes gives the per-unit-area decrease in volume of dispersed phase due to DI coalescence:

$$Q = -\frac{dV}{dt} = \int_0^\infty vk(v)f(v)dv \quad . \tag{6}$$

To simplify this expression, we distinguish between the drop size distribution f(v) for drops at the interface and the drop size distribution g(v) of drops DI-coalescing per unit area per second. The two distributions are not necessarily the same since drops of some sizes may be coalescing faster than those of other sizes. One may, therefore, have an average drop volume $\bar{v}_f$ of drops at the interface which is different from the average drop volume $\bar{v}_g$ of drops undergoing DI coalescence. These averages are defined, respectively, as:

$$\bar{v}_f = \frac{\int_o^\infty vf(v)dv}{\int_o^\infty f(v)dv} \quad \text{and} \tag{7}$$

$$\bar{v}_g = \frac{\int_o^\infty vg(v)dv}{\int_o^\infty g(v)dv} \quad . \tag{8}$$

For a given drop volume v, recall that the number of drops DI-coalescing per unit area per second is k(v)dn or k(v)f(v)dv. Thus, g(v) = k(v)f(v) and eq. 8 may be rewritten:

$$\bar{v}_g = \frac{\int_o^\infty vk(v)f(v)dv}{\int_o^\infty k(v)f(v)dv} \quad . \tag{9}$$

Combining eqs. 3, 6, and 9 gives an expression for dispersed-phase throughput based on the total number of drops coalescing per unit area per second:

$$Q = \bar{v}_g \int_o^\infty k(v)f(v)dv = -\left(\frac{dN}{dt}\right)_{DI} \bar{v}_g \quad . \tag{10}$$

Substituting eq. 5 into eq. 10 yields the simple expression given by Barnea and Mizrahi (7):

$$Q = \bar{k}n\bar{v}_g \quad . \tag{11}$$

Thus, the dispersed-phase throughput equals the product of the average DI coalescence frequency, number of drops per unit area, and average drop volume of DI-coalescing drops.

Experimentally, it is convenient to directly measure Q, $\bar{v}_f$, and n, while measurement of $\bar{k}$ (from eq. 5) and $\bar{v}_g$ is more difficult owing to the problem of distinguishing reliably between disappearance of droplets due to DI coalescence and disappearance due to interdrop coalescence. Hence, we introduce a new related quantity $\bar{k}'$ which we call the average DI coalescence rate, defined according to

$$\bar{k}' = \frac{\int_0^\infty k(v)vf(v)dv}{\int_0^\infty vf(v)dv} \quad . \tag{12}$$

As in eq. 4, we are averaging k(v) over a distribution, except that in eq. 12 the distribution function is vf(v) instead of f(v) alone. Whereas the differential quantity f(v)dv gives the number of drops of volume v, vf(v)dv gives the combined volume of the drops of volume v. Substituting eqs. 6, 7, and 1 into eq. 12 gives the relation

$$Q = \bar{k}' n \bar{v}_f \quad , \tag{13}$$

which contains easily measurable experimental variables.

The distinction between eqs. 11 and 13 is subtle, yet the two expressions are strictly different. In eq. 13, the quantity $n\bar{v}_f$ corresponds to the total volume of drops directly adjacent to a unit area of interface. Thus, we refer to $n\bar{v}_f$ as "available volume" since it is the only volume of dispersed phase (per unit area) subject to DI coalescence at any given instant. The quantity $\bar{k}'$, therefore, represents the number of available volumes undergoing DI coalescence per second as contrasted with $\bar{k}$, representing the fraction of the number of drops adjacent to the interface which coalesce per second.

Both $\bar{k}$ and $\bar{k}'$ appear to be useful quantities. Conversion from one to the other is made by substituting eq. 11 into eq. 13:

$$\bar{k}' = \frac{\bar{v}_g}{\bar{v}_f} \bar{k} \quad . \tag{14}$$

The conversion requires, in essence, that one must know how the coalescence frequency k(v) varies with drop volume. At present, the relationship between k(v) and v must be regarded as unknown (5,6). From the theoretical point of view, $\bar{k}$ is useful because it most easily relates to average DI coalescence time defined as $\bar{\tau} = 1/\bar{k}$. However, without knowing or assuming a functional dependence between k(v) and v, $\bar{k}$ cannot be used to exactly predict

throughput. In the simplest approximation, k(v) is taken to be constant over all drop volumes. Consequently, $\bar{k}' \sim \bar{k}$ and $\bar{v}_f \sim \bar{v}_g$, and the distinction between $\bar{k}'$ and $\bar{k}$ vanishes. This would appear to be a reasonable approximation for relatively narrow drop size distributions.

Up to this point, the discussion has applied generally to either batch or continuous-flow systems. In each case, dispersed-phase throughput Q is readily measurable, though in slightly different form. In continuous flow, Q is simply the dispersed-phase volume flow rate per unit area (or linear flow rate). Batch systems, however, differ in that the disengaged dispersed phase remains stationary while the major interface moves. Assuming a settler with constant cross-sectional area, the dispersed-phase throughput Q may be obtained as the absolute value of the time derivative $\frac{dh}{dt}$ of the vertical height h of the major interface relative to an arbitrary reference level (see Fig. 1). Thus, for batch experiments, eq. 13 becomes

$$\bar{k}' = \left|\frac{dh}{dt}\right| \frac{1}{n\bar{v}_f} \quad . \tag{15}$$

Note that available volume may be viewed simply as the distance the major interface would move if all the drops adjacent to the interface coalesced at once. This equation will be useful in the experimental measurement of average DI coalescence rate.

EXPERIMENTAL SECTION

Chemicals

Tri-n-octylamine (Aldrich Chemical Co., 97%) was distilled using a Consolidated Vacuum Corp. Centrifugal Molecular Still, Type CMS-5 and converted to the chloride salt by shaking with 1 M HCl (Fisher reagent). The wet, liquid TOA·HCl was dried until solidified by rotary evaporation of the excess water under vacuum. Further purification was carried out by fractional crystallization

of 210 g of the solid from purified acetone (Burdick & Jackson Laboratories) to yield 36 g (17%) of snow-white crystals.

Water was purified by double distillation (first out of alkaline $KMnO_4$) using conventional Pyrex glass stills equipped with 50-cm quartz-packed columns. HCl (Baker "Ultrex") was used as received. To remove interface-active impurities, 4 L of purified o-xylene (Burdick & Jackson Laboratories) was passed through a column of 150 g activated alumina (Fisher) and 100 g activated silica gel (Baker). LiCl (Fisher reagent) was recrystallized three times from water.

The organic phase in the study was 0.1 M TOA·HCl in o-xylene, and the aqueous phase was 0.1 M HCl, 0.9 M LiCl. The choice of this particular system was guided by several factors. The amine extractant TOA is commercially important (13,14) and has high solubility as the chloride salt in o-xylene without the need for modifier. All reagents are either readily purified or available in high purity. Further, many basic studies of the chemical behavior of TOA and related amines in aromatic diluents using various aqueous acids have been reported in the literature to guide interpretation of results. We found it necessary to employ high-ionic-strength systems (which are more realistic from a practical viewpoint) to avoid the haze in the aqueous phase associated with low ionic strengths.

Equipment

The phase disengagement cell was designed to meet a number of requirements:

1. distortion-free observation of dispersion from the side and bottom,
2. minimum wall area,
3. reasonably flat interfacial area,
4. vortex-free mixing,
5. conventional mixer configuration (15),
6. noncontaminating construction materials (all glass and Teflon), and
7. temperature control.

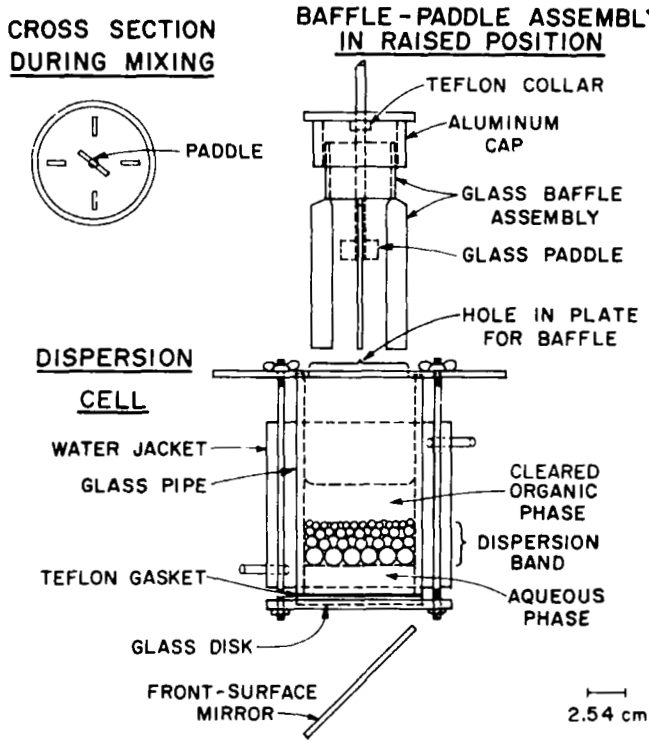

FIGURE 2. Batch Dispersion Cell (to scale). For clarity, the baffle-paddle assembly is shown completely removed from the cell.

As shown in Fig. 2, the body of the cell was constructed of Pyrex glass pipe (5-mm wall thickness, 7.49 cm i.d.) ground flat at either end. Using an intervening Teflon gasket (0.6-mm thickness), the cylinder was clamped to a flat Pyrex glass disk. A water jacket sealed to the back half of the glass pipe with silicone rubber afforded a limited means of temperature control (±1°C).

By means of the stainless steel plate, the cell was positioned between the two upright posts of the motor stand. The variable-speed motor (Electro-Craft Corp. Motomatic Motor Generator with Cole Parmer Master Servodyne controller) was free to slide vertically on the stand, aided by a pulley and counterweight. By means of a tight-fitting Teflon collar on the paddle shaft inside the aluminum cap, the whole paddle/baffle assembly could be

lifted from the cell as one unit when the motor was raised. The cross-sectional geometry of the cell showing the Pyrex glass paddle and baffles is diagrammed in Fig. 2. To permit possible scale-up or modeling, we are working toward a conventional mixing configuration (15) consistent with other design constraints. However, for the present experiment, we employed a paddle for simplicity instead of the preferred six-bladed turbine. Vortexing was effectively eliminated with this design up to a rotor speed of 2000 rpm.

The optical system consisted of a Nikon SMZ-10 Stereo Microscope, Hitachi Model HV-176 CCTV Camera (vidicon tube), Hitachi Video Monitor Model VM-906A, and NEC Videocassette Recorder Model VC-9307E (3/4-in. tape). The microscope was mounted with the optical axis aligned horizontally, and a front-surface mirror oriented 45° to the optical axis allowed the dispersion to be viewed from the bottom of the cell. A 0.5X auxiliary objective lens gave the microscope an effective working distance of approximately 15 cm. The video camera was mounted on the phototube of the microscope via a 5X relay lens. To calibrate the system, the image of a steel rule (0.5-mm increments) was recorded on videocassette tape and measured on playback from the screen of the TV monitor. Over the zoom range of the microscope, effective magnification factors of 7 to 43 were realized. The precision errors due to distortion (±5%), parallax effect on the monitor, and focusing combined to give an estimated overall measurement precision of ±10%.

Procedures

Before the experiment, the two phases were contacted by slow stirring for 1 h and passed through a fritted-glass filter ("medium" porosity: 10-15 μm). Data were collected in a series of runs at 25(±1)°C using a single phase ratio of 0.94:1 (160 mL aqueous plus 170 mL organic) and a stirring speed of 1250 rpm (sufficient to ensure complete dispersion). To initiate a run, the

paddle was briefly positioned in the organic phase to create an organic-continuous dispersion followed by a 3-min mixing period with the paddle at the midpoint of the dispersion. The phase disengagement period began with mixer power cutoff followed by rapid braking of the rotor and hoisting the motor and paddle/baffle assembly.

During the phase disengagement period, the drops at the center of the major interface were simultaneously observed on the CCTV monitor and recorded on videocassette tape. Fourteen runs were made at magnifications of 7.2, 10.7, 21.5, and 42.9. Since the major interface moved upward during phase disengagement, the microscope focus required continual readjustment during each run as did the lighting. It was found that the lighting was particularly critical to the quality of the observed and recorded images and that optimum results could be obtained by directing the beam of light from the side at an acute angle with respect to the plane of the interface. Two ordinary microscope lamps were used.

In a separate series of runs, the changing positions of the major interface and sedimentation boundary were observed through the side of the cell using a cathetometer (Gaertner Scientific Corp.) reading to within 0.05 mm. Since only three readings could be taken in one run, 25 runs were required to plot the dispersion band profile.

Data Handling

Drop diameters were obtained over the course of complete separation of the phases at 10 individual times. Using the still-frame feature of the videocassette recorder, the drop diameters at a particular time were traced by hand onto a plastic transparency fixed to the CCTV monitor screen. To avoid bias, all drops with center points within a given rectangular area A (see Fig. 1) were measured to the nearest millimeter. The volume-average drop diameter $\bar{d}$ was computed, assuming spherical shapes, using the formula

$$\bar{d} = \left(\frac{1}{n_A} \sum_{i=1}^{n_A} d_i^3 \right)^{1/3} , \qquad (16)$$

where n_A is the total number of drops counted in the rectangular area A. The number of drops per unit area follows as $n = n_A/A$. To minimize statistical error, up to approximately 300 drops were analyzed for any one time using eq. 16. Standard error of the mean value $\bar{d}$ was determined by the usual differential method for calculating propagation of errors (16):

$$\sigma_{\bar{d}} = \frac{1}{3} \bar{d}^{-2} \sqrt{\frac{\sum_{i=o}^{n_A} \left(d_i^3 - \bar{d}^3 \right)^2}{n_A (n_A - 1)}} . \qquad (17)$$

The actual scatter of the drop diameters about the mean is given by

$$\sigma_d = \sigma_{\bar{d}} \sqrt{n_A} . \qquad (18)$$

Statistical analysis of the data was performed using the ORNL computer facility after manually inputting the drop sizes.

Examination of the recorded videomicrographic images of the drops at the major interface showed that the drop outlines were circular to a good approximation over the entire range of drop sizes observed. Thus, any error due to treating the drops as spheres would have to result from vertical distortion. Equilibrium shapes of drops resting at interfaces have been calculated by Princen (17). For single drops under conditions frequently encountered in solvent extraction (i.e., interfacial tension >10 mN/m^2 and density difference $\sim$0.2 g/cm^3), the measured drop diameter is accurate to within ±5% for drops up to 2.8 mm as compared with a sphere of equivalent volume. However, in compact dispersions, drops effectively distort against a much smaller density difference due to the constraining influence of neighboring drops. Using an effective density difference of 0.02 g/cm^3

(assuming a holdup fraction of 0.90), we estimate the distortion error to be less than ±5% for drops up to 8.8 mm, covering the entire range of drop sizes studied here.

RESULTS AND DISCUSSION

Dispersion Band Profile

Figure 3A shows the dispersion band profile (plot of dispersion-band boundary positions vs time). The cell bottom is

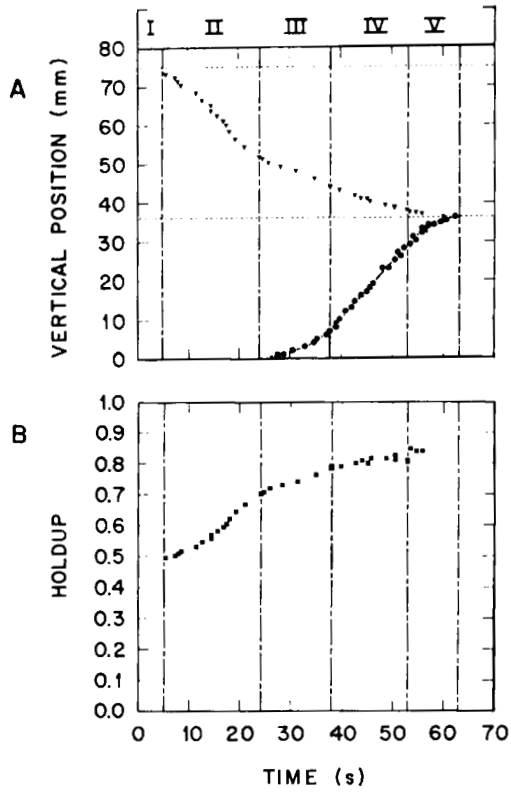

FIGURE 3. Dispersion Band Profile (A) and Holdup (B) Versus Time. The plots are broken into 5 sequential stages (see Table 1). ▼ - sedimentation boundary. ● - major interface. ■ - holdup.

taken to be the reference height (h = 0), and dotted lines denote the levels of the bulk aqueous/organic and organic/air interfaces. Since the dispersion was mixed in the organic-continuous mode, the lower set of points corresponds to the rising position h of the major interface. These points were smoothed using a computer-generated spline curve-fitting routine (18) (solid line) to give a typical S-shaped curve. Based on the scatter about this curve, the reproducibility of the experiment over many runs was ±0.5 mm, or ±1.4% of the total travel of the major interface. Considering the erratic behavior reported frequently in the literature, the high run-to-run reproducibility observed here is remarkable. We attribute it to the use of pure chemicals and noncontaminating cell construction materials.

To test the nature of possible wall effects in the experiment (e.g., rapid drop-wall coalescence), a series of runs was made using a thin Teflon lining in the cell in the form of Teflon sheet (0.25 mm thickness). Except for the initial 5 mm rise of the major interface, the respective dispersion band profiles for Teflon vs glass wall overlapped within experimental error. The initial difference is attributable to the difference in curvature of the interface at the wall of the cell. Due to contact angle differences, the curvature is concave downward with the Teflon wall and concave upward with the glass wall. Thus, a slight artifactual discrepancy arises when the position of h is defined as the level of the midpoint of the interface. In any case, this effect had negligible influence on the later course of phase disengagement, and the results reported involved no Teflon liner since the glass wall was regarded as giving the more reliable data.

As pointed out by Assenov and Slater (19), the dispersion band profile in Fig. 3A may be broken into a number of stages. The stages we have identified from Fig. 3 are listed in Table 1. After power cutoff at the mixer occurs (t = 0s), a brief period of approximately 5 s ensues during which the turbulence in the system decays as indicated by the cessation of swirling motion. In the next stage, the sedimentation boundary undergoes its most rapid

TABLE 1

Batch Phase Disengagement Stages

Time (s)	Stage	Description
0		Power cutoff to mixer
0-5	I	Decay of turbulence
5-24	II	Sedimentation
24-38	III	Increasing throughput
38-53	IV	Rapid, steady throughput
53-63	V	Termination
63		Break

decline, whereas virtually no movement of the major interface occurs. Thus, stage II most conspicuously involves sedimentation-compaction of the dispersion band as the holdup fraction (i.e., the combined volume of dispersed phase divided by total volume of the dispersion band) increases from its initial value of 0.48 to 0.70 at 24 s. During stage III, the throughput as given by the slope $\frac{dh}{dt}$ of the position h of the major interface increases. Stage IV is marked by an approximately linear increase in h with time. Finally, at the maximum holdup of 0.84 in stage V, throughput decreases as the dispersion band shrinks down to the last layer of drops. As given by the intersection of the sedimentation boundary and major interface in Fig. 3A, the break occurred at 63 s, though a number of scattered drops lingered for approximately 10 s afterward.

Except for our addition of stage V to account for the often-observed "tailing-off" of batch phase disengagement profiles, our designations of stages are in agreement with those of Assenov and Slater (19). Similar patterns can also be seen in the batch

results of other workers, although some significant variation in the relative duration of the stages exists (3,6,20,21).

Drop Size Data

Volume-average drop diameters $\bar{d}$ of drops at the major interface as calculated using eq. 16 are plotted in Fig. 4A on a logarithmic scale vs time. The error bars represent the precision (standard deviation $\sigma_{\bar{d}}$ of the mean $\bar{d}$) of the measurement computed from eq. 17. The plot indicates an exponential increase in drop diameter

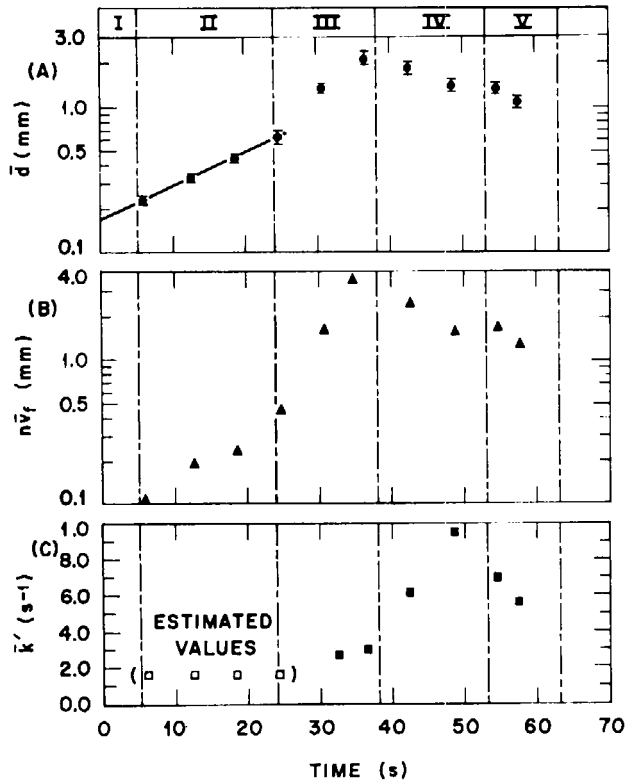

FIGURE 4. Volume-Average Drop Diameter (A), Available Volume (B), and Average DI Coalescence Rate (C) Versus Time. Note that both $\bar{d}$ and $n\bar{v}_f$ are plotted on logarithmic scales. As in Fig. 3, the time scale has been broken into 5 stages.

in stage II followed by an even more rapid increase in drop size in stage III. Maximum drop size occurs at the onset of stage IV, after which the drop size steadily decreases. Table 2 lists these data together with statistical information, packing data, and computational parameters.

Especially striking during the playback of the videorecorded runs is the change in the distribution of drop diameters with time. A formal analysis of the distributions is beyond the scope of this paper and has not yet been made, but qualitatively, the trends are evident in the maximum and minimum diameters (d_{max} and d_{min}) and the overall scatter (σ_d defined in eq. 18) listed in Table 2. Initially relatively narrow, the drop size distribution widens to cover a maximum range of 1.5 orders of magnitude, tapering off gradually thereafter.

Drop size distribution influences the efficiency of drop packing (22) and therefore influences the number of drops (n) per unit area and available volume ($n\bar{v}_f$). For the simplest case of equal-sized drops packed in a tight hexagonal layer, elementary geometrical considerations dictate that n is inversely proportional to the drop diameter squared: $n = 0.907/(\frac{\pi}{4}d^2)$. (The factor 0.907 is the maximum fractional part of a given area that can be covered with equal-sized circles.) Since $\bar{v}_f = \frac{\pi}{6}d^3$, we have $n\bar{v}_f = 0.605d$. Available volume (units are in mm) is therefore expected to increase experimentally in approximate proportion to average drop diameter, assuming tight packing and a narrow range of drop sizes. Table 2 and Fig. 4B show that available volume indeed follows much the same pattern observed for average drop diameter. However, the values for $n\bar{v}_f$ fall in the wide range 0.4 $\bar{d}$ to 1.6 $\bar{d}$, indicating significant differences in packing over the course of the experiment. Values of less than 0.6 $\bar{d}$ observed in stage II presumably indicate somewhat inefficient packing, but as the distribution widens, smaller drops may begin to fill interstitial holes left by larger drops. Thus, available volume rapidly increases throughout stages II and III to a maximum at the point of the widest distribution.

TABLE 2

DI Coalescence Data

t (s)	d_{min} (mm)	d_{max} (mm)	$\bar{d} \pm \sigma_{\bar{d}}$ (mm)	σ_d (mm)	n_A (No. drops)	$n \times 10^2$ (No. drops/cm^2)	$n\bar{v}_f$ (mm)	$\frac{dh}{dt}$ (mm/s)	$\bar{k}'$ (s^{-1})
6.0	0.11	0.32	0.23 ± 0.01	0.05	80	1600	0.10	(0.02)*	(0.16)*
12.6	0.18	0.53	0.34 ± 0.01	0.09	51	939	0.19	(0.03)*	(0.16)*
18.6	0.19	0.80	0.44 ± 0.02	0.15	101	508	0.23	(0.04)*	(0.16)*
24.6	0.23	1.27	0.63 ± 0.02	0.32	182	347	0.45	(0.07)*	(0.16)*
30.6	0.23	4.50	1.36 ± 0.11	1.47	182	120	1.60	0.43	0.27
36.6	0.28	8.42	2.12 ± 0.26	3.86	229	71	3.51	1.04	0.30
42.6	0.28	6.46	1.87 ± 0.19	2.71	200	69	2.34	1.45	0.62
48.6	0.28	4.40	1.41 ± 0.11	1.79	258	102	1.51	1.44	0.95
54.6	0.28	5.33	1.36 ± 0.12	2.00	281	124	1.64	1.14	0.70
57.6	0.23	3.37	1.07 ± 0.11	1.15	120	188	1.22	0.70	0.57

*Estimated values

DI Coalescence Rate

We make direct use of available volume in eq. 15 for the direct determination of the average DI coalescence rate $\bar{k}'$. Needed in the calculation is the slope $\frac{dh}{dt}$, which was taken from the smoothed curve in Fig. 3A for the respective times at which the available volumes were found. The results are listed in Table 2 and plotted in Fig. 4C.

It is evident that the shape of the major interface profile is influenced not only by changing drop size and packing, but also by changing DI coalescence rate $\bar{k}'$. For ease of comparison of the different curves, the smoothed shapes of the plots in Figs. 3 and 4 are combined into one master plot in Fig. 5. Since the movement of the major interface was not observed in stage II, direct measurement of $\bar{k}'$ could not be made for this stage. However, to

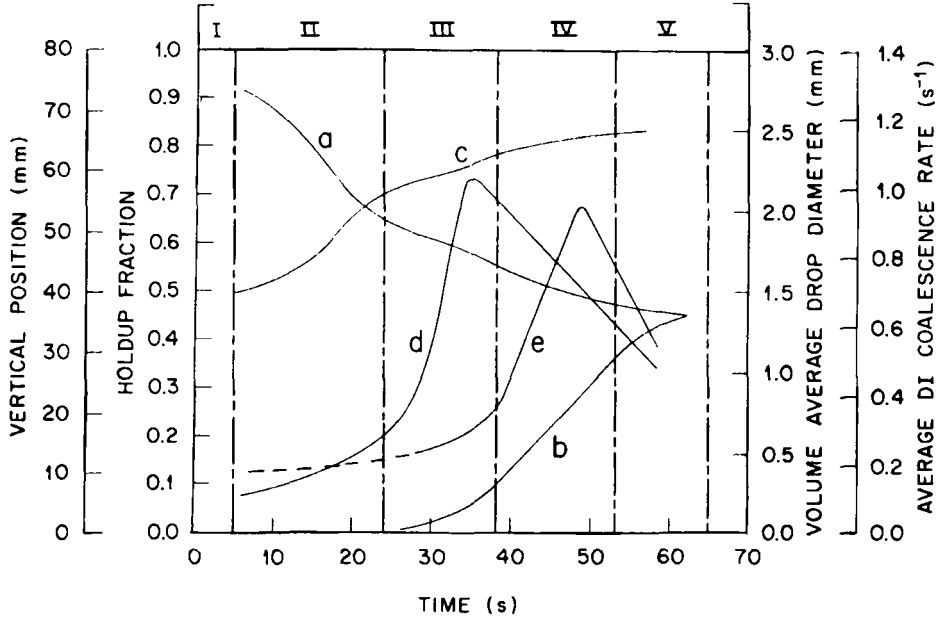

FIGURE 5. Master Plot of (a) Sedimentation Boundary Profile, (b) Major Interface Profile, (c) Holdup, (d) Volume-Average Drop Diameter, and (e) Average DI Coalescence Rate.

account for the negligible throughput in stage II, the value of $\bar{k}'$ must be relatively low as it is in stage III. According to the discussion given later, $\bar{k}'$ may be approximately constant in stage II with a value of approximately 0.16 s^{-1} as indicated by the parenthesized points in Fig. 4C and dashed line in Fig. 5. In stage III, the increased throughput occurs primarily due to increased available volume with little increase in $\bar{k}'$. However, the decreasing available volume in stage IV requires that the average DI coalescence rate must increase to account for the approximately linear throughput. During stage V, both $n\bar{v}_f$ and $\bar{k}'$ decrease, causing the tailing-off of the dispersion band profile.

Two factors are likely to be of importance in explaining the variation in $\bar{k}'$: drop size (6) and interdroplet squeezing forces (12). Based on the noncorrespondence in the peaks in the plots of $\bar{d}$ and $\bar{k}'$ vs time (see Fig. 5), it is obvious that the squeezing forces must influence $\bar{k}'$ strongly, whatever the effect of drop size may be. Hartland and Vohra (12) have presented calculations predicting that coalescence rates increase in close-packed dispersions as squeezing due to the weight of upper drops increases. Accordingly, they account for the tailing-off of the dispersion band profile (i.e., decreasing throughput or slope $\frac{dh}{dt}$) in the later stages of batch phase disengagement in terms of the decreasing thickness (and therefore weight) of the compact dispersion band. Qualitatively, our results appear to reflect this type of behavior. In the latter half of the experiment, the dispersion band takes on its most compact form (highest holdup) as sedimentation-packing processes come to an end, and the highest values of $\bar{k}'$ are observed. Tailing-off of the dispersion band indeed appears to be caused, in part, by decreasing average DI coalescence rate. We plan to assess the role of squeezing more quantitatively in future work by making a careful study of dispersion band structure.

Stage II Model

Interdrop Coalescence. The variation in drop size contains useful information about interdrop coalescence, especially during

stage II where the exponential drop size growth suggests a simple growth mechanism. Early in stage II, a compact bed of drops presumably begins to build up by sedimentation on the major interface (initially at h = o). For convenience, we divide the bed into arbitrarily small layers of equal thickness. As DI coalescence occurs, these layers are sequentially removed from the bed, enabling us to see layers that were originally deposited progressively farther above the interface. As a rough estimate, if holdup in the bed is 0.67 and the major interface rises a total of 1 mm in stage II, then at the end of stage II, we are observing drops that were deposited only 1.5 mm back from the interface. To a good approximation, the layers in this thin, 1.5-mm zone may be assumed to have the same age and the same initial average drop size since the deposition time of the zone must be short.

A model given by Hartland and Vohra (10) predicts the exponential growth in drop diameter subject to the following conditions: (1) all layers have identical drop size distribution, (2) holdup in each layer remains constant, (3) coalescence frequency is a constant independent of drop size, squeezing, or time, and (4) drop shape is spherical. In terms of average interdrop coalescence frequency $\bar{k}_{DD}$ (in place of average interdrop coalescence time, equal to $1/\bar{k}_{DD}$), the model gives the expression

$$\bar{d} = \bar{d}_o e^{\frac{1}{6}\bar{k}_{DD}t} \quad , \tag{19}$$

where $\bar{d}_o$ is the average drop diameter at t = o. The average interdrop (DD) coalescence frequency $\bar{k}_{DD}$ is defined as the fraction of the number of drops in the compact bed which DD-coalesce per second. Taking the logarithm of eq. 19 and applying the resulting expression in a linear least squares analysis of the drop diameters in stage II gives $\bar{k}_{DD} = 0.32\ s^{-1}$ and $\bar{d}_o = 0.17$ mm. The fitted straight line is shown in Fig. 4A. Therefore, eq. 19 appears to describe the initial behavior of the drop sizes at the interface. In later stages, sedimentation rate becomes particularly important as it affects the effective length of time the layers of drops will reside in the compact zone before reaching the interface.

DI coalescence. Since the assumption of constant $\bar{k}_{DD}$ in stage II led to the correct prediction of exponential drop growth, the assumption of constant average DI coalescence frequency $\bar{k} \sim \bar{k}'$ follows as a reasonable approximation for estimation of $\bar{k}'$ in stage II. Hence, the integrated form of eq. 15 becomes

$$h = \bar{k}' \int_{t_o}^{t} n\bar{v}_f dt \quad , \tag{20}$$

where t_o is the time at which DI coalescence begins (h = o). An analytical expression for $\bar{v}_f$ as a function of time can be obtained from eq. 19, but an explicit form for n is unknown (22). Therefore, we graphically integrated the available volume $n\bar{v}_f$ (from Table 2 or Fig. 4B) from 5 to 27.6 s, taking t_o as the approximate time of decay of turbulence. Using the value h = 0.95 mm at t = 27.6 s gives $\bar{k}' = 0.16\ s^{-1}$. This value appears to be reasonable on the basis of the observed trend in the directly measured values (Fig. 4C).

As a rate process, phase disengagement reflects the combined effects of sedimentation, drop-drop coalescence, and drop-interface coalescence, all occurring together and mutually interacting (7). Therefore, a clear-cut distinction as to a rate-limiting step is not meaningful. In the experiment we have just described, it is qualitatively clear that each of these component processes has an important effect on the resultant throughput observed. At present, however, the lack of a comprehensive quantitative model makes a more quantitative comparison of the relative importance of these component processes inaccessible.

SUMMARY

A promising new approach to the measurement of coalescence in liquid/liquid phase disengagement has been presented. New quantities including available volume and average drop-interface coalescence rate ($\bar{k}'$) have been defined, leading to a relation between drop-interface coalescence rate and dispersed-phase throughput.

An experimental method has been developed to measure $\bar{k}'$ in small-scale batch tests. The method utilizes videomicrography to determine drop size distribution and packing density (n) of drops at the major (coalescing) interface. To calculate $\bar{k}'$ at various times in the batch experiment, these data are combined with throughput measurements taken from an analysis of the dispersion band profile.

A batch experiment involving the tertiary amine extractant TOA was performed and analyzed to demonstrate the potential of the experimental approach and to initiate future investigations into chemical influences on coalescence rates in solvent extraction systems. High run-to-run reproducibility in organic-continuous phase disengagement was achieved by the use of high-purity chemicals and noncontaminating construction materials. Wall effects were found to be of only minor significance. Throughput was shown to be affected by drop size growth behavior and changing drop size distribution via their effects on available volume. In addition, the drop-interface coalescence rate $\bar{k}'$, itself, was found to be variable with values in the range 0.16 to 0.95 s^{-1}. The variation in $\bar{k}'$ is thought to arise from changing interdrop "squeezing" effects in the compact zone of the dispersion band in addition to a possible dependence of $\bar{k}'$ on drop size distribution. Overall, the behavior of the system can be described in terms of five sequential stages based on throughput, drop growth, and drop-interface coalescence rate.

NOMENCLATURE

A	rectangular area in which drops were counted at a particular time
d	drop diameter
d_i	diameter of the $i^{\underline{th}}$ drop
$\bar{d}$	volume-average drop diameter
d_{max}, d_{min}	respective maximum and minimum first-layer drop diameters observed at time t

$\bar{d}_o$	average first-layer drop diameter at t = o
f(v)	distribution function of first-layer drops per unit area of interface
g(v)	distribution function of first-layer drops DI-coalescing per unit area per second
h	vertical position (height) of the major interface relative to the bottom of the cell
k(v)	DI coalescence frequency of drops of volume v
$\bar{k}$	average DI coalescence frequency (averaged over the number distribution function f(v))
$\bar{k}'$	average DI coalescence rate (averaged over the volume distribution function vf(v))
$\bar{k}_{DD}$	average interdrop coalescence frequency
n	number of drops per unit area adjacent to the interface (first-layer drops)
n_A	number of first-layer drops in area A
N	number of drops per unit area in the dispersion band
Q	volume rate of throughput per unit area
σ_d	standard deviation of the scatter of drop diameters about the volume-average drop diameter
$\sigma_{\bar{d}}$	standard error of the volume-average drop diameter
t	time
t_o	time at which DI coalescence begins
$\bar{\tau}$	average DI coalescence time ($\bar{\tau} = \frac{1}{\bar{k}}$)
v	drop volume of a first-layer drop
V	combined volume of drops in the dispersed phase per unit area
$\bar{v}_f$	average volume of first-layer drops
$\bar{v}_g$	average volume of DI-coalescing first-layer drops

ACKNOWLEDGMENTS

This work was supported by the Division of Chemical Sciences, U.S. Department of Energy under Contract W-7405-eng-26 with the Union Carbide Corporation. We would also like to thank C. F. Coleman for his valuable suggestions during the course of the work and J. R. Knight for assistance with computer programming and assembling the experimental apparatus.

REFERENCES

1. B. A. Moyer and W. J. McDowell, Sep. Sci. Technol. 16(9), 1261 (1981).

2. A. D. Ryon and R. S. Lowrie, *Experimental Basis for the Design of Mixer Settlers for the Amex Solvent Extraction Process*, Report ORNL-3381, Oak Ridge National Laboratory, April 19, 1963.

3. K. A. Allen and W. J. McDowell, *Emulsion Stabilization by Silicic Acid*, Report ORNL-2771, Oak Ridge National Laboratory, Aug. 17, 1959.

4. P. Sherman, ed., *Emulsion Science*, Academic Press, New York, 1968.

5. E. Barnea, Hydrometallurgy 5, 15 (1979); 127 (1980).

6. S. Vijayan and A. B. Ponter, Chem. Ing. Tech. 47, 748 (1975).

7. E. Barnea and J. Mizrahi, Trans. Inst. Chem. Engrs. 53, pp 61-69; pp 70-74; pp 75-82; pp 83-92 (1975).

8. G. V. Jeffreys, G. A. Davies, and K. Pitt, AIChE Journal 16(5), 823 (1970).

9. S. Vijayan and A. B. Ponter, Proceedings of the International Solvent Extraction Conference, Lyon, 1974, G. V. Jeffreys, ed., Vol. 1, Society of Chemical Industry, London, 1974; pp 591-641.

10. S. Hartland and D. K. Vohra, Chem. Ing. Tech. 50, 673 (1978).

11. A. M. S. Vieler, D. Glasser, and A. W. Bryson, Proceedings of the International Solvent Extraction Conference, Toronto, 1977, The Canadian Institute of Mining and Metallurgy, 1979.

12. S. Hartland and D. K. Vohra, J. Coll. Interface Sci. 77(2), 295 (1980).

13. C. F. Coleman, K. B. Brown, J. G. Moore, and D. J. Crouse, Ind. Eng. Chem. 50, 1756 (1958).

14. G. M. Ritcey and A. W. Ashbrook, *Solvent Extraction/Principles and Applications to Process Metallurgy*, Part II, Elsevier, New York, 1980.

15. F. A. Holland and F. S. Chapman, *Liquid Mixing and Processing in Stirred Tanks*, Reinhold Publishing Corp., New York, 1966.

16. P. R. Bevington, *Data Reduction and Error Analysis for the Physical Sciences*, McGraw-Hill Book Company, New York, 1969.

17. H. M. Princen, J. Coll. Sci. 18, 178 (1963).

18. DISPLA program, Integrated Software Systems Corporation, San Diego, CA.

19. A. Assenov and M. J. Slater, Hydrometallurgy 2, 157 (1976).

20. J. Golob and R. Modic, Trans. Inst. Chem. Eng. 55, 207 (1977).

21. J. C. Godfrey, D. K. Chang-Kakoti, M. J. Slater, and S. Tharmalingam, Proceedings of the International Solvent Extraction Conference, Toronto, 1977, The Canadian Institute of Mining and Metallurgy, 1979.

22. J. A. Dodds, J. Coll. Interface Sci. 77(2), 317 (1980).